Inversion of irradiance and remote sensing reflectance in shallow water between 400 and 800 nm for calculations of water and bottom properties

Andreas Albert and Peter Gege

What we believe to be a new inversion procedure for multi- and hyperspectral data in shallow water, represented by the subsurface irradiance and remote sensing reflectance spectra, was developed based on analytical equations by using the method of nonlinear curve fitting. The iteration starts using an automatic determination of the initial values of the fit parameters: concentration of phytoplankton and suspended matter, absorption of gelbstoff, bottom depth, and the fractions of up to six bottom types. Initial values of the bottom depth and suspended matter concentration are estimated analytically. Phytoplankton concentration and gelbstoff absorption are initially calculated by the method of nested intervals. A sensitivity analysis was made to estimate the accuracy of the entire inversion procedure including model error, error propagation, and influence of instrument characteristics such as noise, and radiometric and spectral resolution. The entire inversion technique is included in a public-domain software (WASI) to provide a fast and user-friendly tool of forward and inverse modeling. © 2006 Optical Society of America

OCIS codes: 010.4450, 280.0280.

1. Introduction

The subsurface irradiance and remote sensing reflectances, R and R_{rs}, are wavelength-dependent functions of absorption $a(\lambda)$ and backscattering $b_b(\lambda)$, and strongly influenced by substances suspended and dissolved in water. Additionally, in shallow water areas, the detected signal is remarkably affected by the light reflected at the bottom. At some spectral regions, different water constituents and the bottom can influence the optical signal in the same manner, making it difficult to distinguish each effect.

So-called forward models were developed (first for optically deep water) based on the radiative transfer in the water, where the reflected signal is calculated as a function of the optical properties of the water and the water constituents. Different approaches exist for solving the radiative transfer equation and modeling the light field under water. Most common are the Monte Carlo method,[1–3] the invariant embedding technique,[4,5] the matrix operator method,[6,7] and the finite-element method.[8,9]

Forward models are useful for the study of the light field under different conditions of the optical properties. The determination of unknown model parameters from a measured spectrum, for example, the concentrations of water constituents, bottom depth, and bottom characteristics like submersed vegetation type, is called inversion. To solve this problem, several approaches exist to date, which are based on a neural network,[10] principal components,[11] and nonlinear optimization.[12,13] What kind of solution is the best to choose depends on several factors such as computing time, accuracy, application to regional or global scales, and the number of spectral channels and unknown parameters. Here the nonlinear optimization technique combined with analytical equations is chosen, since this technique provides fast calculation, simple adaptation of new optical properties, and the physical interpretation of all steps.

2. Analytical Model

The basis of this paper are analytical models of subsurface irradiance reflectance (R) and remote sensing

When this research was performed, A. Albert and P. Gege (peter.gege@dlr.de) were with the Department of Marine Remote Sensing, Institute of Remote Sensing Technology, German Aerospace Center (DLR), Muenchener Strasse 20, D-82234 Wessling, Germany. A. Albert (andreas.albert@gsf.de) is now with the Department of Environmental Engineering, Institute of Soil Ecology, National Research Center for Environment and Health (GSF), Ingolstaedter Landstrasse 1, D-85764 Neuherberg, Germany.

	R	R_{rs}
A_1	1.0546	1.1576
A_2	0.9755	1.0389 sr^{-1}
κ_0	1.0546	1.0546
$\kappa_{1,W}$	1.9991	3.5421
$\kappa_{2,W}$	0.2995	−0.2786
$\kappa_{1,B}$	1.2441	2.2658
$\kappa_{2,B}$	0.5182	0.0577
p_1	0.1034	0.0512 sr^{-1}
p_2	3.3586	4.6659
p_3	−6.5358	−7.8387
p_4	4.6638	5.4571
p_5	2.4121	0.1098
p_6 (s/m)	−0.0005	−0.0044
p_7	—	0.4021

reflectance (R_{rs}) spectra in deep and shallow water
that were developed and validated using longtime
experimental data from Lake Constance.[14–16] The
model equations are summarized briefly. Absorption
a is parameterized as the sum of the absorption of
water, phytoplankton, and gelbstoff (yellow sub-
stances), $a(\lambda) = a_W(\lambda) + a_P{}^*(\lambda)C_P + a_Y(440 \text{ nm})$
$\exp[-0.014(\lambda - 440 \text{ nm})]$, with the specific absorp-
tion of phytoplankton $a_P{}^*(\lambda)$ (Ref. 15) and its concen-
tration C_P. The backscattering coefficient b_b is
expressed as the sum of the backscattering coefficient
of water and a wavelength-independent backscatter-
ing coefficient of suspended particles, $b_b(\lambda)$
$= \frac{1}{2} b_W(\lambda) + b_{b,X}{}^*C_X$, with a specific backscattering
coefficient of suspended matter $b_{b,X}{}^* = 0.0086 \text{ m}^2/\text{g}$
(Ref. 15) and its concentration C_X.

Parameterizations of R and R_{rs} were developed by
Albert and Mobley[16] covering a wide range of concen-
trations. They systematically investigated the influ-
ence of inherent optical properties of the water and
bottom characteristics on R and R_{rs} in deep and shal-
low water. Analytical equations were obtained by re-
gression analysis of about 1400 spectra simulated
with Hydrolight,[5] which is used as the reference
model. The following analytical equations for R and
R_{rs}, depending on absorption a, backscattering b_b,
surface wind speed u, subsurface solar zenith angle
θ_s, subsurface viewing angle θ_v, and the bottom albedo
R_B at depth z_B were derived:

$$R = R_\infty\{1 - A_1 \exp[-(K_d + K_{u,W})z_B]\} + A_2 R_B$$
$$\times \exp\{-(K_d + K_{u,B})z_B\}, \quad (1)$$

$$R_{rs} = R_{rs,\infty}\{1 - A_{rs,1} \exp[-(K_d + k_{u,W})z_B]\}$$
$$+ A_{rs,2} \frac{R_B}{\pi} \exp[-(K_d + k_{u,B})z_B], \quad (2)$$

with empirical coefficients A_i and $A_{rs,i}$ listed in Table
1. The downward and upward diffuse attenuation
coefficients K_d, $K_{u,W}$, and $K_{u,B}$ are given by

$$K_d = \kappa_0 \frac{a + b_b}{\cos \theta_s}, \quad (3)$$

$$K_{u,W} = (a + b_b)(1 + \omega_b)^{\kappa_{1,W}}\left(1 + \frac{\kappa_{2,W}}{\cos \theta_s}\right), \quad (4)$$

$$K_{u,B} = (a + b_b)(1 + \omega_b)^{\kappa_{1,B}}\left(1 + \frac{\kappa_{2,B}}{\cos \theta_s}\right). \quad (5)$$

The attenuation coefficients of the two upwelling ra-
diance components from the water and the bottom
are $k_{u,W} = K_{u,W}/\cos \theta_v$ and $k_{u,B} = K_{u,B}/\cos \theta_v$, respec-
tively. The coefficients κ_i are listed in Table 1. R_∞
$= f^\circ \omega_b$ and $R_{rs,\infty} = f^\uparrow \omega_b$ are the irradiance and remote
sensing reflectance of optically deep water, respec-
tively, with the backscattering albedo $\omega_b = b_b/(a
+ b_b)$. The f factors developed also by regression anal-
ysis of the Hydrolight simulations are given by

$$f^\circ = p_1(1 + p_2\omega_b + p_3\omega_b{}^2 + p_4\omega_b{}^3)$$
$$\times \left(1 + p_5 \frac{1}{\cos \theta_s}\right)(1 + p_6 u), \quad (6)$$

$$f^\uparrow = p_{rs,1}(1 + p_{rs,2}\omega_b + p_{rs,3}\omega_b{}^2 + p_{rs,4}\omega_b{}^3)$$
$$\times \left(1 + p_{rs,5} \frac{1}{\cos \theta_s}\right)(1 + p_{rs,6}u)\left(1 + p_{rs,7} \frac{1}{\cos \theta_v}\right),$$
$$(7)$$

The values of the empirical coefficients p_i and $p_{rs,i}$ are
listed in Table 1. These analytical equations can cal-
culate R and R_{rs} with a relative mean error of 3%
approximately 10^6 times faster compared to Hydro-
light; the time of a single spectrum is approximately
0.1 s (550 MHz processor Pentium III, calculations in
steps of 1 nm between 400 and 800 nm). The de-
scribed analytical equations build the basis of the
inversion. Because R and R_{rs} are parameterized as a
function of a and b_b, the model is independent of the
optical model describing a and b_b.

3. Inversion

Inverse modeling is the determination of parameters
for a given irradiance reflectance or remote sensing
reflectance spectrum. The number of parameters,
which are estimated by inversion and called fit pa-
rameters, depends on the preknowledge about the
situation. In the case of shallow water, the determin-
able parameters are the concentrations of the water
constituents: phytoplankton, suspended matter, and
gelbstoff, and the bottom depth and the bottom type.
The technique of getting the unknown parameters for
a spectrum is briefly described in the following. More
details are explained in Refs. 17 and 18.

A. Curve Fitting and Search Algorithm
The fit parameters are determined iteratively using
the method of nonlinear curve fitting. In the first
iteration, a model spectrum is calculated using initial

values for the fit parameters. This model spectrum is compared with the input spectrum from a measurement or simulation by calculating the residuum as a measure of correspondence. The residuum Δ is calculated as

$$\Delta = \frac{1}{N_\lambda} \sum_{i=1}^{N_\lambda} g_i \, |X_{0,i} - X_i|^2, \qquad (8)$$

with the number of spectral channels N_λ, the input values $X_{0,i}$, and the fitted values X_i of the spectrum of irradiance or remote sensing reflectance. g_i is the weighting factor of a spectral channel. The classical least-squares fit is given for $g_i = 1$ at all wavelengths. Then, in the further iterations, the values of the fit parameters are altered, resulting in altered model curves X_i and altered residuals. The g_i are not changed during inversion. The procedure is stopped after the best fit between calculated and measured spectrum has been found, which corresponds to the minimum residuum. The parameter values that were used in the step with the smallest residuum are the results.

Since there exists an infinite number of possible parameter combinations, an effective algorithm of the iteration process has to be used to select a new set of parameter values from the previous sets. Here, the Simplex algorithm is used,[19,20] which is implemented in the software tool Water Colour Simulator (WASI).[18,21] It has two advantages compared to other customary algorithms such as Newton–Ralphson and Levenberg–Marquardt: it always converges, and it is fast, since no matrix operations are required.

The Simplex algorithm can be described as follows. A virtual space of $M + 1$ dimensions is constructed, where M dimensions represent the M fit parameters and one dimension is the residuum. Each model curve corresponds to one point in that space. The set of all possible model curves obtained by all combinations of parameter values forms an M dimensional surface. That point on the surface where the residuum is minimal represents the solution of the fit problem. The Simplex can be compared to a spider that crawls on the surface searching for the minimum. It consists of $M + 1$ legs, where each leg (vertex) represents a model curve that has already been calculated. The decision regarding which set of parameter values is chosen in the next step (i.e., where the Simplex moves to) is made according to a strategy that includes four new positions calculated by reflection, contraction, expansion, and shrinkage. Not all of these positions are always calculated. They are tested in this order, and the first position is taken where the new vertex is better than the old. Usually the Simplex is trapped in a minimum after less than $20 \, M^2$ iterations.[20] However, if the surface contains local minima, the Simplex may be captured in one of these. In such cases it is important to start the search at a point not too far away from the global minimum. The methodology of the determination of suitable start values is explained in Subsection 3.B.
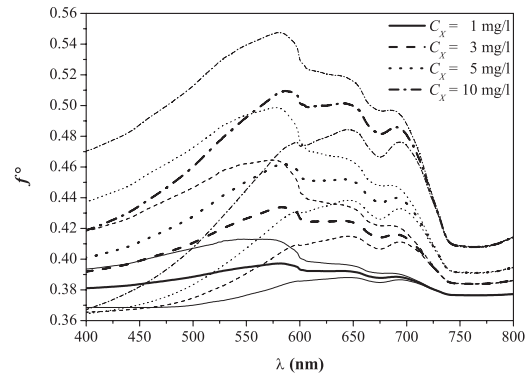

Fig. 1. Variability of the factor f° of Eq. (6). The thick curves represent the average values for the given concentration of suspended matter and for $0.5 \leq C_P \leq 20.0 \, \mu g/l$ and $0.1 \leq a_Y(\lambda_0) \leq 5.0 \, m^{-1}$. The thin curves are the mean plus and minus one standard deviation.

B. Determination of Initial Values

Before the main inversion starts, it is necessary to estimate initial values of the unknown parameters. The strategy of finding initial values as accurate as possible is important to the success of finding the best fit of the input spectra. The following paragraphs explain briefly the determination of the initial values of the bottom depth z_B, the suspended matter concentration C_X, the phytoplankton concentration C_P, and the gelbstoff absorption $a_Y(\lambda_0)$ at $\lambda_0 = 440$ nm. The fastest estimation is realized by using analytical equations. These are obtained by solving the expressions of the irradiance and remote sensing reflectance for the desired parameter. Due to the structure of Eqs. (1)–(7), this is only possible using approximations and special wavelengths.

A general difficulty is the parameterization of the f factors of Eqs. (6) and (7). They include implicitly the concentrations of the water constituents through the absorption and backscattering coefficients. Thus the f factors depend on wavelength. To solve the irradiance and remote sensing reflectance equations for absorption or backscattering a wavelength is chosen, where the f factors are relatively constant over a wide range of water constituent concentrations. Figure 1 shows the variability of the factor f° from 400 to 800 nm for moderate concentrations of suspended matter (1, 3, 5, and 10 mg/l) and for $0.5 \leq C_P \leq 20.0 \, \mu g/l$ and $0.1 \leq a_Y(\lambda_0) \leq 5.0 \, m^{-1}$. The subsurface solar zenith angle was 30° and the subsurface viewing angle was zero for $f^\uparrow$. The influence of the wind speed was ignored, $u = 0$. The curves show clearly the strong influence of absorption by phytoplankton and gelbstoff in the blue and green below 600 nm. In this spectral region the f factors vary by approximately 5% for low concentrations of suspended matter and more than 12% for concentrations of greater than 10 mg/l. Due to the decreasing influence of the absorption of phytoplankton and gelbstoff, the variability of f° and $f^\uparrow$ decreases to approximately 3% for wavelengths above 600 nm and below 1% from 700 nm onward. The f factors do not vary between 700 and 800 nm and are nearly
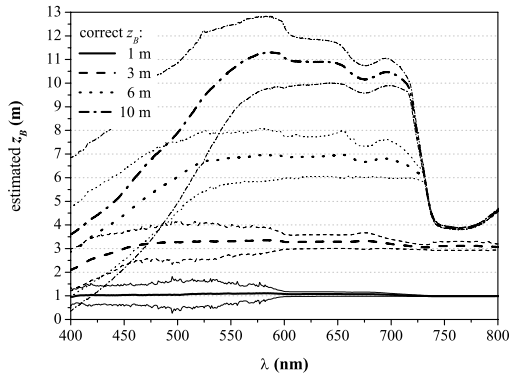
Fig. 2. Bottom depth estimated by Eq. (9) for varying concentrations of $0.5 \le C_P \le 20.0$ µg/l, $0.5 \le C_X \le 10.0$ mg/l, and $0.1 \le a_Y(\lambda_0) \le 5.0$ m^{-1} above sediment and macrophytes. The bottom albedo is assumed to be known during the calculations. Solid curves: mean; dashed curves: intervals given by the standard deviation.
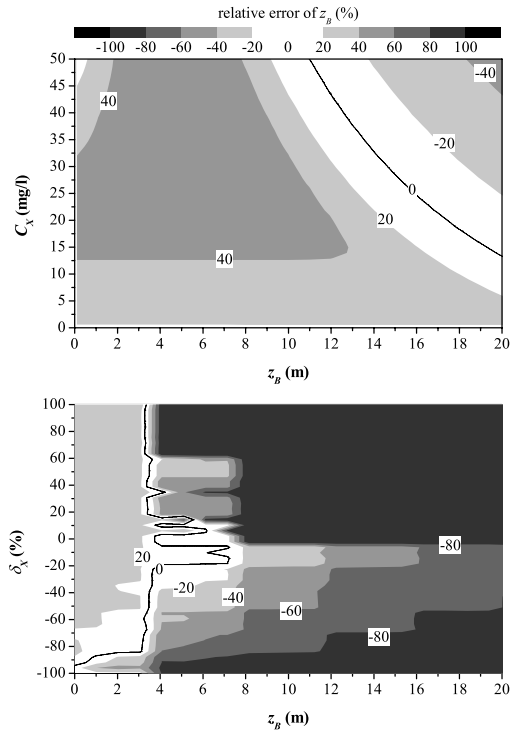

Fig. 3. Relative error of the bottom depth estimated using Eq. (9) depending on the concentration of suspended matter (top) and the relative error of C_X (bottom) above macrophytes: $C_P = 2$ µg/l and $a_Y (440$ nm$) = 0.3$ m^{-1}. The dependence on the relative error of C_X was calculated for $C_X = 2$ mg/l. The subsurface solar zenith angle was 30°.

constant from 750 to 800 nm for a fixed concentration of suspended matter. This spectral region provides the best choice of determining parameters linked to backscattering.[22]

1. Bottom Depth

Analytical equations of z_B can be determined from Eqs. (1) and (2), if no distinction is made between the upward and the downward attenuation coefficients. Setting the upward diffuse attenuation coefficients, $K_{u,W}$ and $K_{u,B}$, equal to the downward diffuse attenuation, K_d, results in an underestimation of the reflectances of approximately 15% for natural waters.[23] But for estimation of the initial value of the bottom depth, such an error is acceptable. Using that approximation yields the following equations of z_B for R and R_{rs}:

$$z_B = \frac{1}{2K_d} \ln\left(\frac{A_1 R_\infty - A_2 R_B}{R_\infty - R}\right), \qquad (9)$$

$$z_B = \frac{1}{K_d\left(1 + \frac{1}{\cos\theta_v}\right)} \ln\left(\frac{A_{rs,1}R_{rs,\infty} - A_{rs,2}\frac{R_B}{\pi}}{R_{rs,\infty} - R_{rs}}\right). \qquad (10)$$

Figure 2 illustrates the accuracy of Eq. (9) from 400 to 800 nm at examples of 1, 3, 6, and 10 m bottom depth and concentrations of the water constituents $0.5 \le C_P \le 20.0$ µg/l, $0.5 \le C_X \le 10.0$ mg/l, and $0.1 \le a_Y(\lambda_0) \le 5.0$ m^{-1}. Equation (10) shows the same results and is not presented additionally. *In situ* measured bottom albedo spectra of sediment and macrophytes[16] were used and assumed to be known during the calculations. The curves show that the bottom depth is obtained with little error between 600 and 700 nm. Below 600 nm the high absorption of phytoplankton and gelbstoff causes very large errors. When the bottom depth increases to $z_B > 10$ m, the increasing absorption of the water restricts the estimation to wavelengths below 650 nm (figure not shown). Thus the best-suited wavelength interval to calculate the initial value of the bottom depth is 600–650 nm.

The accuracy of the initial value determination is illustrated at the example of the irradiance reflectance in Fig. 3. The relative error of the bottom depth, $\delta_z = z_B/z_{B,0} - 1$, is plotted depending on C_X (top) and on the relative error of C_X (bottom). For a bottom depth up to 10 m the relative error δ_z is 20%–40% for $C_X < 12$ mg/l and 60% and more for higher concentrations. The error caused by phytoplankton and gelbstoff is below 20% up to a depth of 15 m (Ref. 17) (figure not shown here). The lower panel of Fig. 3 shows for z_B ranging from 0.1 to 20.0 m the relative error of the initial value of z_B depending on the relative error of C_X. The relative error δ_z is generally below 40% for $z_B < 4$ m, except for a high overestimation of the concentration of more than 80%. For greater bottom depths the relative error of the initial value is typically 40%–100%, but can be more. If the suspended matter concentration is underestimated, the bottom depth is underestimated as well.

Summarizing, the initial value determination of z_B using Eqs. (9) and (10) provides acceptable errors especially for a bottom depth lower than 10 m. Large errors in suspended matter determination may cause the failure of the bottom depth estimate if $z_B > 4$ m,

but as shown in Subsection 3.B.2 even analytical equations provide sufficient accuracy of suspended matter concentration. At increasing bottom depth the increasing attenuation of the water body reduces the possibility of estimating bottom depth and therefore bottom type as well.

2. Concentration of Suspended Matter

The initial value of the concentration of suspended matter can also be estimated analytically. As before for the bottom depth, Eqs. (1) and (2) must be simplified: $K_{u,W} = K_{u,B} = K_d$. As shown in Fig. 1, the f factor varies only slightly for wavelengths greater than 750 nm. This is due to the negligible absorption of phytoplankton and gelbstoff in the near infrared,[22] where the total absorption is dominated by the absorption of water. If absorption of phytoplankton and gelbstoff is neglected for $\lambda > 750$ nm, the relative error of $f°$ and $f^\uparrow$ is below 1%. Additionally, the absolute value of backscattering b_b is very low in comparison to the total absorption at this wavelength due to high absorption of pure water. Thus $f°$ and $f^\uparrow$ are approximated to be wavelength-independent and estimated using $\omega_b = \frac{1}{2} b_W/(a_W + \frac{1}{2} b_W)$. The diffuse attenuation coefficients are approximated by $K_{u,W} = K_{u,B} = K_d \approx \kappa_0(a_W + \frac{1}{2} b_W)/\cos\theta_s$. The simplified equations of R and R_{rs} can be solved now analytically for the unknown concentration of suspended matter $C_X = (b_b - \frac{1}{2} b_W)/b_{b,X}*$. The following relations for C_X are obtained by using R and R_{rs}:

$$C_X = \frac{\Re°(a_W + \frac{1}{2} b_W) - \frac{1}{2} b_W}{b_{b,X}*(1 - \Re°)}, \quad (11)$$

$$C_X = \frac{\Re^\uparrow(a_W + \frac{1}{2} b_W) - \frac{1}{2} b_W}{b_{b,X}*(1 - \Re^\uparrow)}, \quad (12)$$

with

$$\Re° \equiv \frac{R - A_2 R_B \exp(-2K_d z_B)}{f°[1 - A_1 \exp(-2K_d z_B)]},$$

$$\Re^\uparrow \equiv \frac{R_{rs} - A_{rs,2}\dfrac{R_B}{\pi} \exp[-K_d(1 + 1/\cos\theta_v)z_B]}{f^\uparrow\{1 - A_{rs,1} \exp[-K_d(1 + 1/\cos\theta_v)z_B]\}}.$$

The relative error $\delta_X = C_X/C_{X,0} - 1$ of the suspended matter concentration was analyzed for C_X from 0.1 to 50.0 mg/l depending on the bottom depth, phytoplankton concentration, gelbstoff absorption, and bottom type.[17] The wavelength for the determination was 760 nm. No dependence on the concentration of phytoplankton and the bottom depth was found for $z_B > 2$ m and only a slight dependence on the gelbstoff absorption. For Eq. (11) the relative error is below 20% for $C_X \leq 5$ mg/l and increases to 40% at $C_X = 25$ mg/l and more than 60% for $C_X \geq 47$ mg/l. For Eq. (12) the relative errors are a bit higher: $<40\%$ at $C_X \leq 17$ mg/l, $<60\%$ at $C_X \leq 30$ mg/l, and $>80\%$

for $C_X \geq 45$ mg/l. At $z_B = 1$ m the relative error of C_X increases to 40% and at a very low bottom depth below 0.5 m δ_X increases to more than 60%.

Summarizing, C_X can be calculated analytically by Eqs. (11) and (12) with sufficient accuracy over a wide range.

3. Concentration of Phytoplankton and Absorption of Gelbstoff

The problem of the determination of initial values for the absorbing water constituents is that Eqs. (1) and (2) cannot be solved analytically for the absorption of phytoplankton and gelbstoff. Thus the sum of the absorption of phytoplankton and gelbstoff, defined as $A(\lambda) \equiv a_P*(\lambda)C_P + a_Y(\lambda_0)\exp[-s_Y(\lambda - \lambda_0)]$, is estimated first. By means of the technique of nested intervals it is possible to find the absorption for all wavelengths by varying $A(\lambda)$ in Eqs. (1) and (2). A starting value $A_0 = 5$ m^{-1} and a step $\Delta = 1$ m^{-1} are chosen to represent the range of the absorption and to converge before the maximum value of iterations $i_{max} = 100$ is reached. The iteration ends either when the relative difference of the reflectance is below a threshold $|\delta|$, which is set to 0.01, or when the number of iterations exceeds i_{max}. The determination of the $i + 1$-value of A is done by the following rule:

$$A_{i+1} = \begin{cases} A_i + \dfrac{\Delta}{i}, & \text{if } \delta < 0 \\[2mm] A_i - \dfrac{\Delta}{i}, & \text{if } \delta > 0 \end{cases}. \quad (13)$$

After the spectrum $A(\lambda)$ is determined by nested intervals, C_P and $a_Y(\lambda_0)$ are estimated using the Simplex algorithm by fitting this spectrum from 400 to 800 nm. The wavelength interval is 5 nm and a maximum number of 10 iterations of the Simplex is chosen, which was found to be sufficient to calculate the initial values of the concentration of phytoplankton and the absorption of gelbstoff.

The efficiency of the method was investigated[17] from 0.1 to 100.0 µg/l for C_P and from 0.01 to 5.0 m^{-1} for $a_Y(\lambda_0)$, $\lambda_0 = 440$ nm. The relative error $\delta_P = C_P/C_{P,0} - 1$ of the initial value of C_P varies for the entire range near zero and increases to approximately 20% only for very low concentrations near 0.1 µg/l. This is the case for all investigated water constituent concentrations, bottom depths, and bottom types. The same is valid for the relative error $\delta_Y = a_Y/a_{Y,0} - 1$ of the initial value of $a_Y(\lambda_0)$.

The influence of errors of the parameters of the water body on the accuracy of C_P and $a_Y(\lambda_0)$ was also analyzed.[17] As shown in Fig. 4, the bottom affects the determination of phytoplankton concentration markedly for $C_P < 10$ µg/l (top) and for $a_Y(\lambda_0) < 0.3$ m^{-1} (bottom). An overestimation of z_B results in an underestimation of C_P and $a_Y(\lambda_0)$, and vice versa, whereas underestimation of z_B is more critical than overestimation: δ_P is nearly 100% if z_B is underestimated by 5%, but is only approximately 60%–80% if z_B is overestimated by 30%; δ_Y is not much affected by
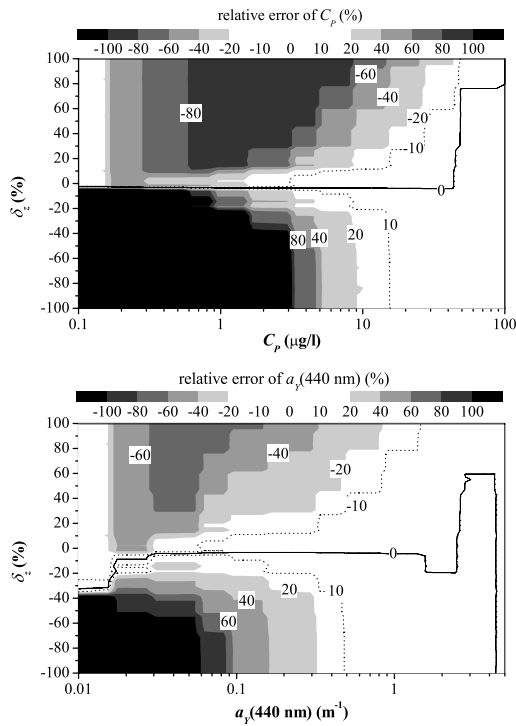
Fig. 4. Relative error of the estimated phytoplankton concentration (top) and gelbstoff absorption (bottom) using nested intervals and the Simplex algorithm depending on the relative error of the bottom depth above macrophytes; if not varied, the values were fixed at $C_P = 2$ µg/l, $C_X = 2$ µg/l, $a_Y (440 \text{ nm}) = 0.3 \text{ m}^{-1}$, and $z_B = 3$ m. The subsurface solar zenith angle was 30°.

an overestimation of z_B, but is >40% if z_B is underestimated by 40%. For increasing phytoplankton concentrations and gelbstoff absorption, the influence of a wrong bottom depth is decreasing due to the increasing optical thickness of the water column.

In general,[17] the influence of an error in z_B, C_X, and R_B decreases for increasing C_P and $a_Y(\lambda_0)$. A 20% overestimation of C_X results in an approximately 100% overestimation of C_P and $a_Y(\lambda_0)$ if $C_P \leq 10$ µg/l and $a_Y(\lambda_0) \leq 0.75 \text{ m}^{-1}$, respectively. But for $C_P \geq 20$ µg/l and $a_Y(\lambda_0) \geq 1.0 \text{ m}^{-1}$ the relative errors δ_P and δ_Y decrease to 40% for the same range of overestimation of C_X. The two parameters C_P and $a_Y(\lambda_0)$ interact inversely: an overestimation of $a_Y(\lambda_0)$ results in an underestimation of C_P, and vice versa.

To conclude, the initial values of C_P and $a_Y(\lambda_0)$ can be derived with sufficient accuracy before starting the main inversion if z_B and C_X are calculated using the methods described above.

4. Areal Fraction of Bottom Albedo

Before the main inversion starts, the user has to select n bottom types in the sensor's field of view. Up to six bottom types can be fitted simultaneously. The areal fraction $f_{a,i}$ of bottom type number i is equal to the percentage coverage of this bottom type for the observed area. If there is no knowledge about the bottom types, the user can select to fit the areal fraction of each bottom type, and the initial values of $f_{a,i}$,

$1 \leq i \leq n$, are assigned as $f_{a,i} = 1/n$. Thus the sum of all fractions is 1. As the experiences from fitting show, this method of assigning the initial values of $f_{a,i}$ is well suited.

C. Precalculation and Prefits

Before the main fit starts, the initial value calculations and some prefits have to be done in a certain order, as explained in the following subsections, and the user has to select an input spectrum of R or R_{rs} and which parameters shall be fitted. For shallow water inversion it is also necessary to select the bottom types, represented by the n bottom albedo spectra $R_{B,i}(\lambda)$. Six different bottom albedos can be chosen from a spectral library included in WASI,[18,21] which can be edited by the user to define his own spectra.

1. Steps of the Initial Value Calculation

The initial estimates of phytoplankton concentration and gelbstoff absorption require knowledge about the bottom depth and the suspended matter concentration. Thus this step is at the end, and the calculations of bottom depth and suspended matter concentration are at the beginning. If z_B and C_X are the fit parameters, then a loop is included to optimize the initial values of z_B and C_X before the initial values of C_P and $a_Y(\lambda_0)$ are derived. This stepwise estimation of the initial values shows the best results.

2. Prefits in the Blue and Near-Infrared Spectra

After the determination of all initial values, the input spectrum is first fitted for infrared wavelengths from 700 to 800 nm and then in the blue from 400 to 500 nm. It is sufficient to use a wavelength interval of 5 nm and to limit the maximum number of iterations to 100. This step improves the initial values of suspended matter concentration, gelbstoff absorption, phytoplankton concentration, and bottom depth.

D. Main Fit

After the initial values are estimated and the prefits in the infrared and blue wavelengths are done, the main fit starts using the input spectrum of the irradiance or remote sensing reflectance. The software WASI (Refs. 18 and 21) allows the user to define the spectral region that is fitted, the spectral data interval or individual spectral channels, and individual weights for each channel. This is useful for suppressing errors from noisy spectral regions and for optimizing computing time. Here the spectra are fitted from 400 to 800 nm using the Simplex algorithm at a wavelength interval of 1 nm. The Simplex is a set of $M + 1$ vectors. Each vector (or vertex) contains the actual values of the M fit parameters and the corresponding residuum. When the fit routine is started, the $M + 1$ vertices are initialized: the fit parameters' initial values and the corresponding residuum form one vertex, the other M vertices are calculated using incremental changes of the initial values. These increments are set to 10% of the initial values. The fit is stopped when either the termination criterion is fulfilled or the maximum number of iterations is

reached. The termination criterion is as follows: the differences between the actual parameter values compared to the step before must be less than a threshold for each parameter. Each parameter has its specific threshold, which is set to 10^{-5} times the initial value. The user defines the maximum number of iterations, which should be set high enough that a forced stop is exceptional.

The accuracy of the inversion technique was investigated for the water constituents concentrations, bottom depth, and bottom coverage. The efficiency of the method is good; the relative error of C_P, C_X, $a_Y(\lambda_0)$ at $\lambda_0 = 440$ nm, z_B, and $f_{a,i}$ is below 0.1% if one parameter is fitted and all other parameters were fixed. More realistic error estimates are obtained by fitting simultaneously more than one parameter. However, the obtained errors are a mixture of errors from the model and error propagation. An analysis of these effects and the resulting errors is given in Section 4 and is presented in detail by Albert.[17]

4. Analysis of Inversion Accuracy

This section discusses the accuracy of the new inversion in shallow water under the influence of the model error itself, the error propagation using several fit parameters, and of sensor characteristics such as signal noise, and radiometric and spectral resolution.

A. Model Error

Differences exist between the (numerical exact) reference model Hydrolight and the analytical shallow water parameterizations,[16,17] which affect the determination of the water and bottom properties by the inversion. To quantify this model error, the spectra of R and R_{rs} were simulated using Hydrolight. These were so-called correct spectra for known values of all model parameters and fitted using the analytical model and the fit strategy described above. The wavelengths from 660 to 715 nm were excluded during the inversion due to the fluorescence of chlorophyll, which was included in the Hydrolight simulations but not in the analytical parameterizations. The relative errors of the fit parameters C_P, C_X, $a_Y(\lambda_0)$, $\lambda_0 = 440$ nm, and z_B were calculated.[17] Some examples that represent typical situations at our test site, Lake Constance, are shown in Fig. 5 for $C_P = 2.0$ µg/l, $C_X = 2.0$ mg/l, $a_Y(\lambda_0) = 0.3$ m^{-1}, and $z_B = 3$ m, if not varied.

The accuracy of the retrieved suspended matter concentration is shown in the upper panel of Fig. 5 as a function of C_X and z_B. C_X is generally underestimated. For $z_B > 2$ m, the relative error of C_X is between 0% and 10%; for $z_B < 2$ m and $C_X < 2.0$ mg/l, the relative error is >10%. The lower panel of Fig. 5 shows the relative error of C_P depending on C_P and z_B. It is <15% for $C_P > 2$ µg/l except for $z_B \geq 10$ m, where the relative error of C_P is >20%. For lower concentrations and increasing z_B the relative error increases up to −40%. This is due to the influence of gelbstoff fluorescence, which increases with bottom depth. Thus the fit compensates the higher reflec-
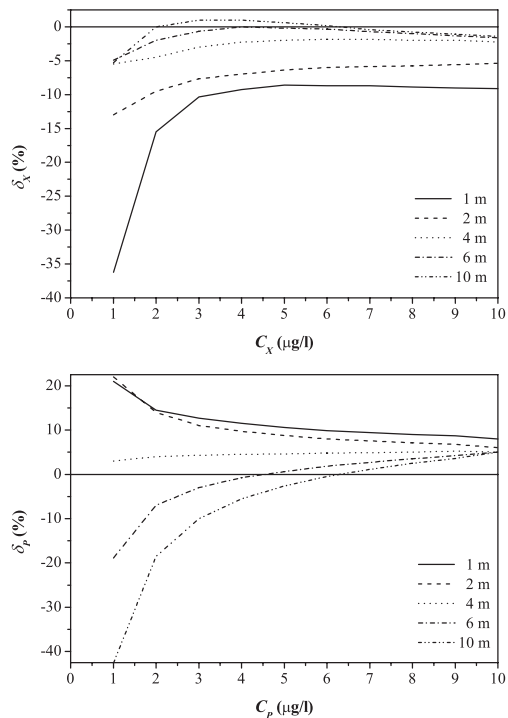

Fig. 5. Relative error of suspended matter (top) and phytoplankton (bottom) concentration resulting from the inversion of the Hydrolight simulated spectra of the irradiance reflectance for different values of the bottom depth above sediment. If not varied, $C_P = 2$ µg/l, $C_X = 2$ mg/l, and a_Y (440 nm) = 0.3 m^{-1} was set.

tance by decreasing the concentrations of the absorbing water constituents. The errors are larger for phytoplankton than for gelbstoff.

The relative error of z_B was investigated from 1 to 10 m depending on C_P, C_X, and $a_Y(\lambda_0)$. The dependence on C_P and C_X is shown in Fig. 6; that on $a_Y(\lambda_0)$ is similar to that on C_P and is not presented here. The results show clearly the limits of detecting the bottom characteristics. The influence of the bottom decreases with increasing optical thickness of the water body, which is coupled to the absorption and scattering. For $1 \leq C_P \leq 10$ µg/l and $0.1 \leq a_Y(\lambda_0) \leq 1.0$ m^{-1}, the relative error of z_B is approximately 5% for $z_B < 5$ m. The greatest impact is due to the amount of suspended matter in the water. Even for $z_B < 5$ m and $C_X \leq 5$ mg/l the relative error increases to 25% for R and 15% for R_{rs}. The influence of phytoplankton and gelbstoff is lower than that of suspended matter. Below 5 m the relative error of z_B is between 0 and 5% and increases for greater bottom depths to 25% and more.

B. Error Propagation

Only one parameter was treated as a fit parameter in Subsection 4.A, but in reality, more than one parameter is unknown and has to be determined. Therefore forward and inverse calculations were made using the analytical model to study the accuracy of the fit parameters if two or more parameters are determined by the inversion technique in shallow water.
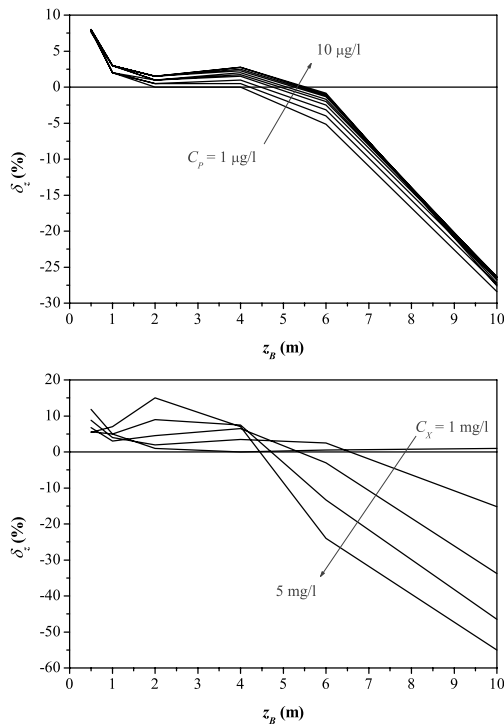
Fig. 6. Relative error of retrieved bottom depth using the Hydrolight spectra of the remote sensing reflectance depending on phytoplankton (top) and suspended matter concentration (bottom) above sediment. If not varied, $C_P = 2$ μg/l, $C_X = 2$ mg/l, and $a_Y(440 \text{ nm}) = 0.3 \text{ m}^{-1}$ was set.
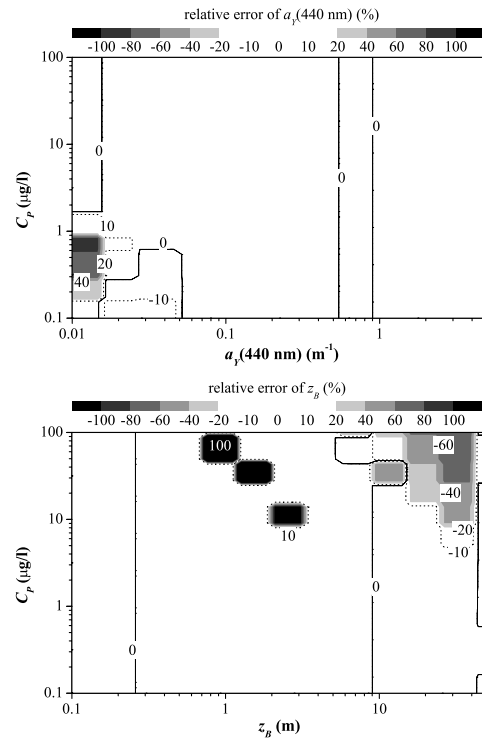

Fig. 7. Relative error of gelbstoff absorption (top) and bottom depth (bottom) for the simultaneous determination of two fit parameters. Fit parameters are a_Y (440 nm) and C_P for the left panel, and z_B and C_P for the right. If not fitted, $C_X = 2.0$ mg/l, a_Y (440 nm) = 0.3 m^{-1}, and $z_B = 3$ m. The bottom type is sediment.

In the case of shallow water remote sensing, C_P, C_X, $a_Y(\lambda_0)$ at $\lambda_0 = 440$ nm, z_B, and $f_{a,i}$ are the unknown parameters. Detailed investigations for deep water were presented by Gege.[24]

Figure 7 shows the relative error of $a_Y(\lambda_0)$ (top) and z_B (bottom) for the case that the respective parameter is estimated by inversion simultaneously with C_P. Not fitted parameters are kept constant at their correct values during the inversion: $C_X = 2.0$ mg/l, $a_Y(\lambda_0) = 0.3$ m^{-1}, and $z_B = 3$ m. The figures were calculated with the bottom-type sediment. The results of calculations with a bottom albedo of macrophytes show the same features and are not displayed. The relative error of $a_Y(\lambda_0)$ is generally below 5%. Exceptions are for a phytoplankton concentration below 1 μg/l in combination with very low gelbstoff absorption below 0.05 m^{-1}. The reason here is the increased influence of the bottom reflectance. The relative error of z_B is generally below 5% for a wide range of C_P and z_B. Only for $C_P > 10$ μg/l in combination with $z_B > 10$ m the relative error of z_B is greater than 50% due to the increasing optical thickness of the water body.

The features of the relative error of C_P are similar to those presented in the upper panel of Fig. 7 (see Ref. 17). The relative error of C_P is below 5% for $C_P > 1.0$ μg/l independent of the second fit parameter. The error increases to 50% and more for lower phytoplankton concentrations and for $C_X < 0.2$ mg/l or $a_Y(\lambda_0) < 0.1$ m^{-1}. This is due to the low optical thick-

ness of the water body and therefore the domination of the bottom reflectance. Low values of C_P, C_X, and $a_Y(\lambda_0)$ change the spectral shape of R and R_{rs} very little and are thus hard to estimate by inversion. The relative error of C_P increases for $C_P < 1$ μg/l and for C_X between 3 and 10 mg/l, but decreases for higher suspended matter concentrations. This can be explained by the decreasing influence of the bottom due to increasing turbidity.

The relative error of C_X is generally very low (0%–5%, figure not shown) if C_X is determined simultaneously with C_P, $a_Y(\lambda_0)$, or z_B. There are only two exceptions of higher relative errors of C_X up to 100%: (i) for $C_P < 0.2$ μg/l in combination with $C_X < 0.2$ mg/l, and (ii) at extremely low bottom depth of $z_B < 0.2$ m.

If the three parameters C_P, C_X, and $a_Y(\lambda_0)$ are determined simultaneously at a fixed bottom depth, their relative errors are very low, i.e., between 0% and 5%. The relative errors decrease with increasing concentrations. The plots are not shown here but are displayed in Ref. 17.

The errors are similar if the bottom depth is a fit parameter together with two water constituent concentrations. The higher the concentration of C_X, the higher the error of z_B, and the lower the bottom depth, the higher the error of C_X. The third fit parameter does not affect the accuracy of z_B and C_X compared to the fit of only z_B and C_X.
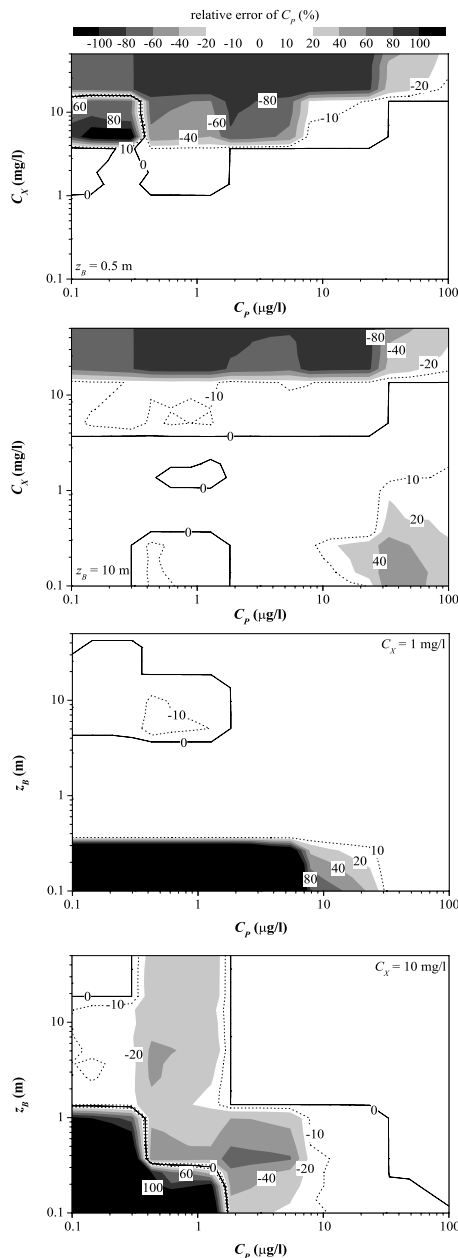
The only complex behavior of error propagation

Fig. 8. Relative error of the phytoplankton concentration for the simultaneous determination of three fit parameters C_P, C_X, and z_B. The correct values of a_Y (440 nm) = 0.3 m^{-1} and the bottom albedo of sediment were fixed during the inversion.

when fitting three parameters simultaneously shows the accuracy of the phytoplankton concentration. These dependences are illustrated in Fig. 8. The main conclusions are as follows: for low and moderate suspended matter concentration, the relative error of C_P is below 5% for shallow water (z_B = 0.5 m), but increases for $C_X > 3$ mg/l. The errors are typically greater than 50% for $C_X > 6$ mg/l. The influence of suspended matter on the phytoplankton concentration decreases if the bottom depth or the concentration of phytoplankton increases. Below a bottom depth of 0.2 m the relative error of C_P is >100%,

Table 2. Water Constituent Concentrations and Bottom Depths Used for Hydrolight Simulations

C_P (µg/l)	1.0	2.0	3.0	4.0	5.0	6.0	7.0	8.0	9.0	10.0
C_X (mg/l)	1.0	2.0	3.0	4.0	5.0	6.0	7.0	8.0	9.0	10.0
$aY(\lambda_0)$ (m^{-1})	0.10	0.20	0.30	0.40	0.50	0.60	0.70	0.80	0.90	1.00
z_B (m)	0.5	1.0	2.0	4.0	6.0	10.0				

except for very high concentrations of 25 µg/l and more.

The accuracy of the determination of the areal fraction of the two bottom types sediment and macrophyte together with the bottom depth was also analyzed.[17] The concentrations of the water constituents were C_P = 2.0 µg/l, C_X = 2.0 mg/l, and $a_Y(\lambda_0) = 0.3$ m^{-1}. The relative error of $f_{a,i}$ is below 5% if $z_B \le 6$ m. The relative error of z_B is also below 5% for $z_B \le 6$ m and increases rapidly for greater bottom depths.

Finally, error propagation was investigated for the simultaneous inversion of the four parameters C_P, C_X, $a_Y(\lambda_0)$, and z_B in combination with the model error. We used 488 Hydrolight simulated spectra typical for Lake Constance as input of the inversion. The range of the varied parameters is listed in Table 2. The mean values of the relative errors δ_P, δ_X, δ_Y, and δ_z and their standard deviations are listed in Table 3. The mean values of the relative errors indicate in most cases a systematic underestimation, but are generally low: the maximum is at 18% for C_P above sediment. In all other cases, the systematic errors are of the order of 2%–12%.

The frequency distributions of the relative errors above macrophytes are shown in Fig. 9. The results above sediment are similar and are not presented here. The relative errors of C_P are distributed most broadly with maxima of ±90% due to the fact that the retrieval of C_P is sensitive and strongly affected by the other parameters and their errors as analyzed in the error propagation study above. Even for the inversion in deep water without the influence of the bottom, the phytoplankton concentration is susceptible to errors of suspended matter concentration and gelbstoff absorption.[24] The distribution of δ_Y is narrow with maximum errors of ±20%. Some outliers occur with higher errors for very low gelbstoff absorp-

Table 3. Mean Values of the Relative Error and Standard Deviations[a]

	$\bar{\delta}_{sed}$ (%)	σ_{sed} (%)	$\bar{\delta}_{mac}$ (%)	σ_{mac} (%)
C_P	−18	35	−8	36
C_X	−11	22	−10	9
a_Y	−2	24	2	13
z_B	−5	20	−12	25

[a]Mean values of the relative error $\bar{\delta}$ and standard deviations σ of C_P, C_X, a_Y (440 nm), and z_B estimated by inversion of 488 Hydrolight simulated spectra for the bottom type sediment (index *sed*) and macrophytes (index *mac*). All four parameters were fitted simultaneously.
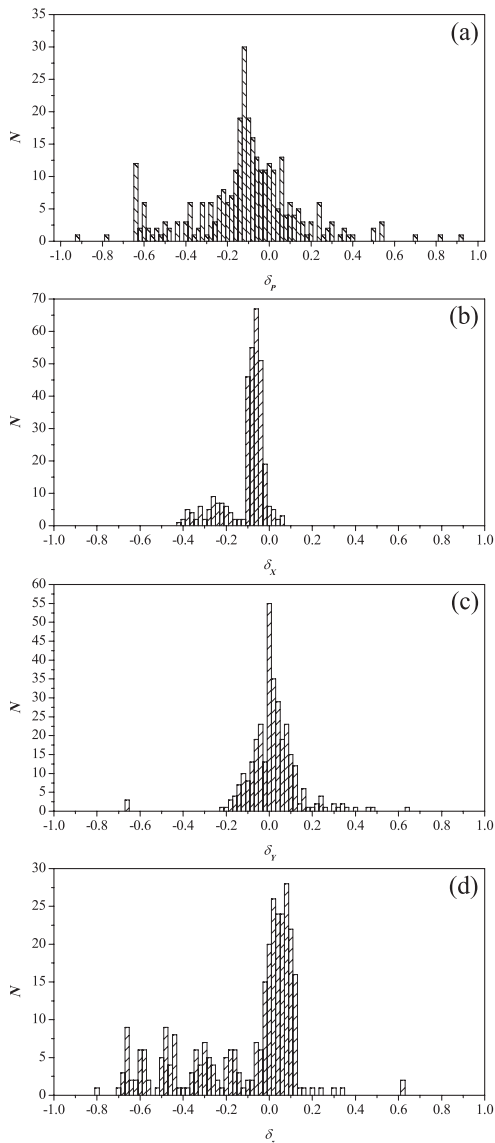
Fig. 9. Frequency distribution of the relative errors of (a) C_P, (b) C_X, (c) (440 nm), and (d) z_B by inversion of the Hydrolight spectra of the remote sensing reflectance and by fitting all four parameters simultaneously. The bottom type was macrophyte.

tion (<0.1 m^{-1}), or due to incorrect estimation of C_P. The relative errors of C_X are distributed from -40% to 10% with the mean peak between $\pm 10\%$. The higher errors from -40% to -20% are owing to values of $C_X < 2$ mg/l for $z_B \leq 1$ m. The distribution of δ_z shows a nonuniform behavior. Besides the strong peak from -10% to 10%, many cases of underestimation up to 70% are recognizable. They appear at high concentrations of the water constituents as explained above.

To summarize the analysis of error propagation: In principle it is feasible to estimate water constituent concentrations and bottom characteristics in shallow waters from subsurface irradiance and remote sensing reflectance spectra. The mean values of the relative errors of the inverted parameters are typically 10%. Water constituent determination gets unreli-

able at very low bottom depth, and bottom depth determination at high optical thickness caused by high water constituent concentrations.

C. Signal Noise and Radiometric and Spectral Resolution

The effect of instrument characteristics on the accuracy of the estimation of parameters by the inversion technique is described in the following. A sensor is characterized by its signal noise δ, radiometric resolution ΔR_{rs}, and spectral resolution $\Delta\lambda$. The software WASI is able to simulate these effects.

For the simulations, the spectral resolution $\Delta\lambda$ was set to 1, 5, 10, and 20 nm. The radiometric resolution was treated as nearly perfect ($\Delta R_{rs} = 10^{-8}$ sr^{-1}) and as a large error source ($\Delta R_{rs} = 10^{-3}$ sr^{-1}), where ΔR_{rs} is the minimum difference in remote sensing reflectance that can be resolved by the instrument. The latter value is realistic for airborne and spaceborne systems.[15,25,26] The simulations for the signal noise considered the sensor characteristic that the shot noise depends on the spectral resolution: The higher the spectral resolution, the higher the shot noise, and vice versa. Thus the signal noise δ was set to 5×10^{-4}, 3×10^{-4}, 2×10^{-4}, and 1×10^{-4} for spectral resolutions of 1, 5, 10, and 20 nm, respectively.[15,25] Ten calculations were made for each parameter combination because signal noise disturbs the spectrum statistically. Calculations with $\Delta\lambda = 1$ nm, $\delta = 0$, and $\Delta R_{rs} = 10^{-8}$ sr^{-1} were used as a reference.

Figure 10 shows the results for C_P and z_B inverting spectra of R_{rs} above sediment and treating a single parameter as unknown. Calculations above macrophytes and retrievals using spectra of R above both bottom types produced similar results[17] and are not shown here. The mean relative errors of C_P, C_X, $a_Y(\lambda_0)$, $\lambda_0 = 440$ nm, and z_B are listed in Table 4. The maximum detectable bottom depth $z_{B,\,max}$ is given as that z_B, from that on δ_z increases rapidly to more than 100%.

The relative error of all parameters is negligible ($<1\%$) and the maximum detectable bottom depth $z_{B,\,max}$ is 20–22 m depending on the bottom type if the spectrum is noise free, the radiometric resolution is 10^{-8} sr^{-1}, and the spectral resolution is 1 nm. When adding statistical signal noise, most of all the bottom depth is affected: $z_{B,\,max}$ decreases to 11–13 m. This is due to the fact that the signal noise disturbs the spectral shape between 600 and 700 nm. The mean relative error of z_B is below 1% when the bottom is detectable. The influence of noise and radiometric and spectral resolution on the concentration of phytoplankton and suspended matter is low for concentrations greater than 1 μg/l and 1 mg/l, respectively. The relative error is below 10% and increases with increasing noise and decreasing radiometric and spectral resolution, especially for concentrations below 0.5 μg/l and 0.5 mg/l, respectively. The relative error of $a_Y(\lambda_0)$ is below 5% and increases for decreasing spectral resolution to approximately 10% over the entire range from 0.01 to 5.00 m^{-1}.
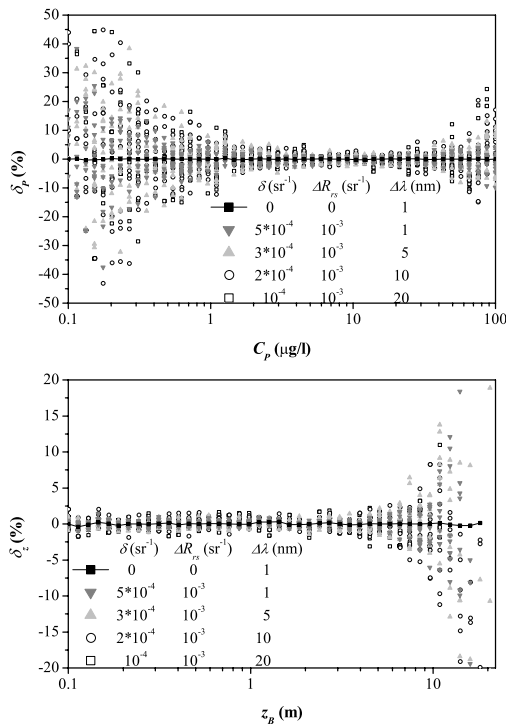
Fig. 10. Relative error of the retrieved phytoplankton concentration (top) and bottom depth (bottom) at the fitting spectra of R_{rs} depending on signal noise δ, radiometric resolution ΔR_{rs}, and spectral resolution $\Delta\lambda$. Not fitted parameters were fixed during the inversion at their correct values $C_P = 2$ μg/l, $C_X = 2$ mg/l, a_Y (440 nm) = 0.3 m^{-1}, and $z_B = 3$ m. The bottom type was sediment.

5. Summary

This study described the development and sensitivity analysis of an inversion technique for optical remote sensing data (400–800 nm) in shallow water.

Analytical parameterizations of the irradiance reflectance and the remote sensing reflectance developed by Albert and Mobley[16] were used. These are approximately 10^6 times faster than the reference model Hydrolight. Based on analytical parameterizations, what we believe to be a new inversion procedure for shallow water applications was developed

and included in the software tool WASI (Refs. 18 and 21) to provide a user-friendly tool for forward and inverse modeling. It is based on the method of non-linear curve fitting and uses the Simplex algorithm.[19,20] The first step is an automatic determination of the initial values of the fit parameters. A new and robust methodology was developed for shallow waters to find the initial values of water constituent concentrations, bottom depth, and areal fractions of up to six different bottom types. The performance of the initial value determination was analyzed in detail for the relevant parameters. The values of the water constituent concentrations, and consequently the inherent optical properties, were varied over a wide range to cover a great variety of waters. The result is that bottom depth and suspended matter concentration can be estimated analytically with an accuracy of approximately 20%–40%, and phytoplankton concentration and gelbstoff absorption by the method of nested intervals with an accuracy of approximately 60%–80%. These accuracies were sufficient for the following main fit by the Simplex algorithm. Although the initial value determination and inversion procedure were developed and tested for conditions at Lake Constance in Germany,[16,17] the technique can be easily adjusted to other water types by changing coefficients, specific optical properties, and bottom conditions.

A sensitivity analysis was made to estimate the accuracy of the entire inversion procedure including model error, error propagation, and influence of the instrument characteristics noise, radiometric, and spectral resolution. Tables 3 and 4 list the resulting mean relative errors and standard deviations of the water constituent concentrations and the bottom depth. Bottom depth and suspended matter concentration can be estimated most accurately, followed by gelbstoff absorption. The determination of phytoplankton concentration is most sensitive. For increasing bottom depth the relative error of z_B increases with higher concentrations of the water constituents. Signal noise and reduced radiometric and spectral resolution increase the errors of the water constituent concentrations and the bottom depth to typically

Table 4. Mean Relative Errors[a]

δ (sr^{-1})	0	5×10^{-4}	3×10^{-4}	2×10^{-4}	10^{-4}
ΔR_{rs} (sr^{-1})	0	1×10^{-3}	1×10^{-3}	1×10^{-3}	1×10^{-3}
$\Delta\lambda$ (nm)	1	1	5	10	20
$\bar{\delta}_P$ (%)	<1	2–3	3–5	4–6	5–6
$\bar{\delta}_X$ (%)	<1	4–5	6–7	7–8	7–8
$\bar{\delta}_Y$ (%)	<1	1	1–2	1–3	2–3
$\bar{\delta}_z$ (%)	<1	<1	<1	<1	<1
$z_{B,\,max}$ (m)	20–22	15–16	14–15	12–14	11–13

[a]Mean relative errors of the phytoplankton concentration ($\bar{\delta}_P$), suspended matter concentration ($\bar{\delta}_X$), gelbstoff absorption ($\bar{\delta}_Y$), and bottom depth ($\bar{\delta}_z$) from inversion depending on signal noise δ, radiometric resolution ΔR_{rs}, and spectral resolution $\Delta\lambda$. Each spectrum of R_{rs} was calculated ten times with a different noise pattern. The ranges of the parameters are $0.1 \leq C_P \leq 100.0$ μg/l, $0.1 \leq C_X \leq 50.0$ mg/l, $0.01 \leq a_Y$ (440 nm) ≤ 5.00 m^{-1}, and 0.1 m $\leq z_B \leq z_{B,max}$, where $z_{B,max}$ denotes the maximum detectable value of the bottom depth (δ_z increases rapidly to >100% for greater bottom depths). If not inverted, the parameters were fixed at their correct values $C_P = 2$ μg/l, $C_X = 2$ mg/l, a_Y (440 nm) = 0.3 m^{-1}, and $z_B = 3$ m. The bottom types were sediment and macrophytes.

10% and restrict the estimation of low water constituent concentrations and the detection of the bottom.

In comparison to other analytical approaches, the performance of the described inversion scheme shows similar results, but for an extended range of concentrations and different kinds of bottom type. For example, Lee et al.[12] calculated the bottom depth with an accuracy of 5%, the phytoplankton absorption with 7%, and the gelbstoff absorption with 7%, but only for a sandy bottom type and a smaller concentration range. The investigations of Mobley et al.[13] using lookup tables calculated by Hydrolight yielded an accuracy of the bottom depth of approximately 10%. Inversion of irradiance and remote sensing reflectance spectra using WASI requires calculation times of the order of a second per spectrum. This is approximately 10^5 times shorter than a calculation of Hydrolight performed on the same computer.

6. Outlook

Investigations are necessary for validation of the new method against *in situ* measurements. Also, the variability of specific optical properties of phytoplankton and suspended particles have to be analyzed carefully in the future to improve the model. Influences of particle size distributions may play an important role especially in shallow water areas. Investigations on the specific optical properties of gelbstoff may improve the results as well.[27,28] The implementation of an analytical model of chlorophyll and gelbstoff fluorescence, as, for example, done by Pozdnyakov et al.,[29] is also expected to improve the accuracy.

References

1. H. Gordon and O. Brown, "Irradiance reflectivity of a flat ocean as a function of its optical properties," Appl. Opt. **12,** 1549–1551 (1973).
2. A. Morel and L. Prieur, "Analysis of variations in ocean color," Limnol. Oceanogr. **22,** 709–722 (1977).
3. J. Kirk, Monte Carlo procedure for simulating the penetration of light into natural waters, CSIRO Division of Plant Industry, Technical Paper **36,** 1–16 (1981).
4. R. Preisendorfer, *Hydrologic Optics* (U.S. Department of Commerce, National Oceanic and Atmospheric Administration, Environmental Research Laboratories, Pacific Marine Environmental Laboratory, 1976).
5. C. Mobley, *Light and Water: Radiative Transfer in Natural Waters* (Academic, 1994).
6. J. Fischer and H. Grassl, "Radiative transfer in an atmosphere-ocean system: an azimuthally dependent matrix-operator approach," Appl. Opt. **23,** 1032–1039 (1984).
7. F. Fell and J. Fischer, "Numerical simulation of the light field in the atmosphere–ocean system using the matrix-operator method," J. Quant. Spectrosc. Radiat. Transfer **69,** 351–388 (2001).
8. V. Kisselev, L. Roberti, and G. Perona, "Finite-element algorithm for radiative transfer in vertically inhomogeneous media: numerical scheme and applications," Appl. Opt. **34,** 8460–8471 (1995).
9. B. Bulgarelli, V. Kisselev, and L. Roberti, "Radiative transfer in the atmosphere–ocean system: the finite-element method," Appl. Opt. **38,** 1530–1542 (1999).
10. R. Doerffer and H. Schiller, "Determination of case 2 water constituents using radiative transfer simulation and its inversion by neural network," in *Proceedings of Ocean Optics XIV Conference, Hawaii, November 10–13,* S. G. Ackleson, ed. (U.S. Office of Naval Research, Ocean, Atmosphere, and Space Science and Technology Department, 1998).
11. H. Krawczyk, A. Neumann, T. Walzel, and G. Zimmermann, "Investigation of interpretation possibilities of spectral high-dimensional measurements by means of principle component analysis: a concept for physical interpretation of those measurements," in *Recent Advances in Sensors, Radiometric Calibration, and Processing of Remotely Sensed Data*, P. S. Chavez, Jr. and R. A. Schowengerdt, eds., Proc. SPIE **1938,** 401–411 (1993).
12. Z. Lee, K. Carder, C. Mobley, R. Steward, and J. Patch, "Hyperspectral remote sensing for shallow waters: 2. Deriving bottom depths and water properties by optimization," Appl. Opt. **38,** 3831–3843 (1999).
13. C. Mobley, L. Sundman, C. Davis, M. Montes, and W. Bissett, "A look-up-table approach to inverting remotely sensed ocean color data," in *Ocean Optics XVI, Santa Fe, USA, 18–22 November, 2002, Proceedings on CD* (U.S. Office of Naval Research, Ocean, Atmosphere, and Space Science and Technology Department, 2002).
14. P. Gege, "Characterization of the phytoplankton in Lake Constance for classification by remote sensing," Arch. Hydrobiol. Spec. Issues Adv. Limnol. **53,** 179–193 (1998).
15. T. Heege, "Flugzeuggestützte Fernerkundung von Wasserinhaltsstoffen im Bodensee," Ph.D. thesis (Institut für Methodik der Fernerkundung, Deutsches Zentrum für Luft- und Raumfahrt Oberpfaffenhofen, 2000).
16. A. Albert and C. Mobley, "An analytical model for subsurface irradiance and remote sensing reflectance in deep and shallow case-2 waters," Opt. Express **11,** 2873–2890 (2003).
17. A. Albert, "Inversion technique for optical remote sensing in shallow water," Ph.D. dissertation (University of Hamburg, Department of Earth Sciences, 2004), http://www.sub.uni-hamburg.de/opus/volltexte/2005/2325/.
18. P. Gege and A. Albert, in *Remote Sensing of Aquatic Coastal Ecosystem Processes*, Vol. 9 of Remote Sensing and Digital Image Processing, L. L. Richardson and E. F. LeDrew, eds. (Springer, 2006), Chap. 4.
19. J. Nelder and R. Mead, "A simplex method for function minimization," Comput. J. **7,** 308–313 (1965).
20. M. Caceci and W. Cacheris, "Fitting curves to data—the simplex algorithm is the answer," Byte Mag. **9**(5), 340–362 (1984).
21. P. Gege, "The water colour simulator WASI: an integrating software tool for analysis and simulation of optical *in situ* spectra," Comput. Geosci. **30,** 523–532 (2004).
22. M. Babin and D. Stramski, "Light absorption by aquatic particles in the near-infrared spectral region," Limnol. Oceanogr. **47,** 911–915 (2002).
23. S. Maritorena, A. Morel, and B. Gentili, "Diffuse reflectance of oceanic shallow waters: influence of water depth and bottom albedo," Limnol. Oceanogr. **39,** 1689–1703 (1994).
24. P. Gege, "Error propagation at inversion of irradiance reflec-

tance spectra in case-2 waters," in *Ocean Optics XVI, Santa Fe, N. Mex., 18–22 November, 2002, Proceedings on CD* (U.S. Office of Naval Research, Ocean, Atmosphere, and Space Science and Technology Department, 2002).

25. J. Schulz, "Systemtechnische Untersuchungen an dem abbildenden Spektrometer ROSIS-01 zur Erfassung und Interpretation der Meeresfarbe," Ph.D. dissertation (Institut für Optoelektronik, Deutsche Forschungsanstalt für Luft- und Raumfahrt Oberpfaffenhofen, 1997).

26. Minimum requirements for an operational ocean-colour sensor for the open ocean, Vol. 1 of Reports of the International Ocean-Colour Coordinating Group (IOCCG, 1998).

27. P. Gege, "Gaussian model for yellow substance absorption spectra," in *Ocean Optics XV, Monaco, France, 16–20 October, 2000, Proceedings on CD* (U.S. Office of Naval Research, Ocean, Atmosphere, and Space Science and Technology Department, 2000).

28. J. Schwarz, P. Kowalczuk, S. Kaczmarek, G. Cota, B. Mitchell, M. Kahru, F. Chavez, A. Cunningham, D. McKee, P. Gege, M. Kishino, D. Phinney, and R. Raine, "Two models for absorption by colored dissolved organic matter (CDOM)," Oceanologia **44,** 209–241 (2002).

29. D. Pozdnyakov, A. Lyaskovsky, H. Grassl, L. Pettersson, and F. Tanis, "Optically shallow waters: modeling of radiometric colour and development of water quality retrieval algorithms," in *Seventh International Conference on Remote Sensing for Marine and Coastal Environments, Miami, Fla., 20–22 May, 2002,* Proceedings on CD (Veridian Systems Division, 2002).